

# Insight into Enzymatic Nitrile Reduction: QM/MM Study of the Catalytic Mechanism of QueF Nitrile Reductase

António J. M. Ribeiro,<sup>†</sup> Lifeng Yang,<sup>‡</sup> Maria J. Ramos,<sup>†</sup> Pedro A. Fernandes,<sup>\*,†</sup> Zhao-Xun Liang,<sup>\*,‡</sup> and Hajime Hirao<sup>\*,§</sup>

<sup>†</sup>UCIBIO, REQUIMTE, Departamento de Química e Bioquímica, Faculdade de Ciências, Universidade do Porto, Rua do Campo Alegre s/n, 4169-007 Porto, Portugal

<sup>‡</sup>Division of Structural Biology & Biochemistry, School of Biological Sciences, Nanyang Technological University, Singapore

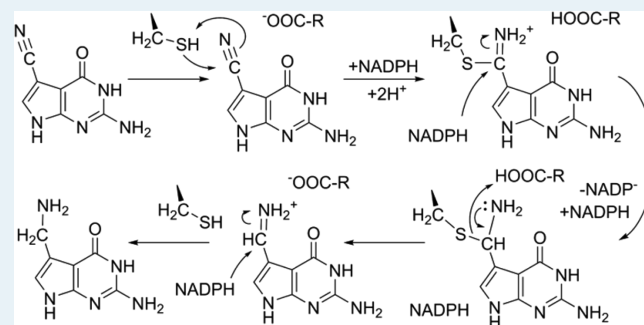
<sup>§</sup>Division of Chemistry and Biological Chemistry, School of Physical and Mathematical Sciences, Nanyang Technological University, 21 Nanyang Link, 637371 Singapore

## Supporting Information

**ABSTRACT:** The NADPH-dependent QueF nitrile reductases catalyze the unprecedented four-electron reduction of nitrile to amine. QueF nitrile reductases can be found in the tRNA biosynthetic pathway of many bacteria and are potential antimicrobial drug targets. QueF enzymes have also attracted great attention as potential industrial biocatalysts for replacing the nitrile-reducing metal hydride catalysts used commonly in the chemical and pharmaceutical industries. Because of their narrow substrate specificity, engineering of the QueF enzymes to generate variants with altered or broadened substrate specificity is crucial for producing practically useful biocatalysts. A better understanding of the catalytic mechanism of

the QueF enzymes would expedite rational inhibitor design and enzyme engineering. In this work, we probed the catalytic mechanism of the *Vibrio cholerae* QueF nitrile reductase by state of the art QM/MM calculations at the ONIOM(B3LYP/6-311+G(2d,2p):AMBER) level. The QM/MM computational results suggest that the nitrile to amine conversion proceeds through four major stages: (a) formation of a C–S covalent bond between the substrate and the catalytic cysteine residue to form the thioimide intermediate, (b) hydride transfer from NADPH to the substrate to generate the thiohemiaminal intermediate, (c) cleavage of the C–S covalent bond to generate the imine intermediate, and (d) second hydride transfer from NADPH to the imine intermediate to generate the final amine product. The free energy barrier for the rate-limiting step, i.e. the second hydride transfer, was found to be 20.8 kcal/mol. The calculated barrier height and the catalytic residues identified as essential for nitrile reduction are in accordance with the currently available experimental data. The knowledge about the transition states, intermediates, and protein conformational changes along the reaction path will be valuable for the design of enzyme inhibitors as well as the engineering of QueF nitrile reductases.

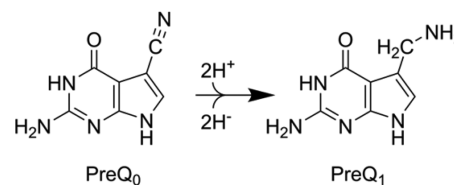
**KEYWORDS:** nitrile reductase, biocatalyst, transition state, enzyme catalysis, covalent intermediate



## 1. INTRODUCTION

QueF nitrile reductases were discovered from the biosynthetic pathway of queuosine (Q), a 7-deazaguanine-modified nucleoside found exclusively at the wobble position of tRNAs. Although Q is crucial for the fidelity and efficiency of translation in both bacteria and eukarya, the Q biosynthetic pathways are only found in bacteria.<sup>1,2</sup> Within the Q-biosynthesizing pathway, QueF catalyzes the NADPH-dependent reduction of the biosynthetic intermediate 7-cyano-7-deazaguanine (preQ<sub>0</sub>) to 7-aminoethyl-7-deazaguanine (preQ<sub>1</sub>) (Scheme 1).<sup>3</sup> Q-containing tRNAs are essential for the expression of the virulence genes of *Shigella flexneri*, without which the bacterium loses its pathogenicity.<sup>4</sup> Because de novo biosynthesis of Q occurs only in bacteria, the Q biosynthetic enzymes such as QueF nitrile reductase are potentially

## Scheme 1. Chemical Reaction Catalyzed by Nitrile Reductase through a Four-Electron Reduction of the Nitrile Group of preQ<sub>0</sub>



Received: March 12, 2015

Revised: May 3, 2015

Published: May 11, 2015

promising targets for the development of new antibacterial compounds. Meanwhile, compounds bearing a nitrile group are common synthetic precursors for obtaining amides, carboxylic acids, and amines in the chemical and pharmaceutical industries. Nitrile hydratases and nitrilases have already been developed successfully as enzyme biocatalysts for the transformation of nitriles into amides and carboxylic acids, respectively.<sup>5–9</sup> However, the nitrile to amine transformations are still catalyzed by using complex metal hydrides, which inevitably generate undesirable byproducts and solvent waste.<sup>10</sup> The unexpected discovery of the QueF family of nitrile reductases raised the hope of developing environmentally sustainable biocatalysts for the nitrile to amine transformation.<sup>10–14</sup>

Biochemical and structural characterization of QueF homologues from *Bacillus subtilis* (*B. subtilis*), *Vibrio cholerae* (*V. cholerae*), *Escherichia coli* (*E. coli*), and *Geobacillus kaustophilus* (*G. kaustophilus*) have yielded valuable insight into the mechanism of nitrile reduction.<sup>15–20</sup> Crystal structures of the QueF homologues from *V. cholerae* and *B. subtilis* have been determined (PDB IDs: 3RJ4, 3BP1, 3UXJ, 3UXV, 4GHM, 4IQI, 4F8B).<sup>15–17</sup> The crystal structures revealed that the QueF enzymes from *V. cholerae* and *B. subtilis* form a homodimer and homodecamer, respectively. The subunit of the dimeric *V. cholerae* QueF adopts a tunneling-fold or T-fold that is composed of four  $\beta$ -strands and two  $\alpha$ -helices.<sup>21</sup> The binding mode of the substrate preQ<sub>0</sub> in the active site has been determined from the crystal structure of the enzyme–substrate complex.<sup>15–18</sup> Although none of the current crystal structures contains the entire NADPH cofactor, which is likely due to the mobility of the nicotinamide group, the position of the nicotinamide group can be inferred from the position of the diphosphate and ribose/adenine moieties. The crystal structures together indicate that the dimeric QueF only binds one NADPH molecule, with the nicotinamide and adenine moieties of the NADPH cofactor situated in the two substrate-binding pockets. As such, the nitrile reduction occurs most probably in only one monomer at a time. The crystal structures of *V. cholerae* QueF also reveal the presence of seven amino acid residues in the first coordination sphere of the substrate preQ<sub>0</sub> (Figure 1).<sup>15–18</sup> The side-chain groups of Glu94, Glu234, and Phe232 and the main-chain groups of Ser95 and Ile93 are directly responsible for the binding of PreQ<sub>0</sub>. The other three residues, Cys194, Asp201, and His233, are positioned next to the nitrile group of PreQ<sub>0</sub>, and it has been suggested that they are the key catalytic residues.<sup>15–17</sup> Most importantly, Cys194 was proposed to function as a nucleophile that attacks the nitrile group to form a thioimide intermediate during catalysis. The involvement of the thioimide intermediate was confirmed by the X-ray crystallographic analysis of the covalent intermediate and the observation that Cys194 can be readily modified by iodoacetamide.<sup>20</sup> Mutagenic studies of *E. coli* QueF showed that only Asp and Cys, which correspond to Asp201 and Cys194 of *V. cholerae* QueF, are essential for catalysis.<sup>13</sup>

The overall mechanism of the nitrile reductase reaction was proposed to include four major stages (Scheme 2): (a) the formation of a C–S covalent bond between the substrate and the Cys194 residue, (b) the transfer of a hydride ion from NADPH to the Cys-tethered intermediate, (c) the cleavage of the C–S covalent bond and formation of an imine intermediate, and (d) the transfer of a hydride ion from a second NADPH molecule to the imine intermediate.<sup>10</sup> With

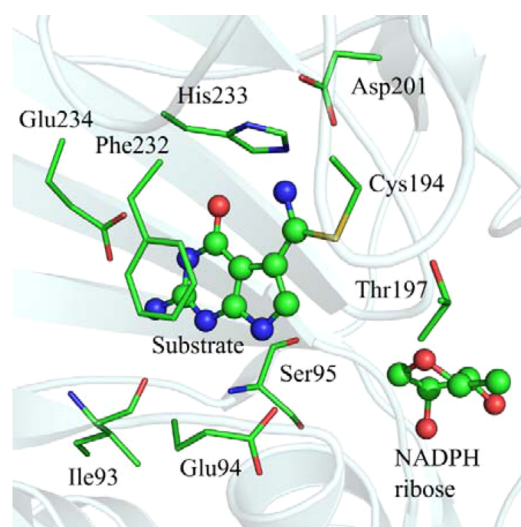


**Figure 1.** Schematic illustration of the active site of *V. cholerae* QueF nitrile reductase (PDB code 3UXJ). Catalytic and substrate-binding residues are shown in a stick representation. The covalently attached PreQ<sub>0</sub> and the ribose group of NADPH are shown in a ball and stick representation.

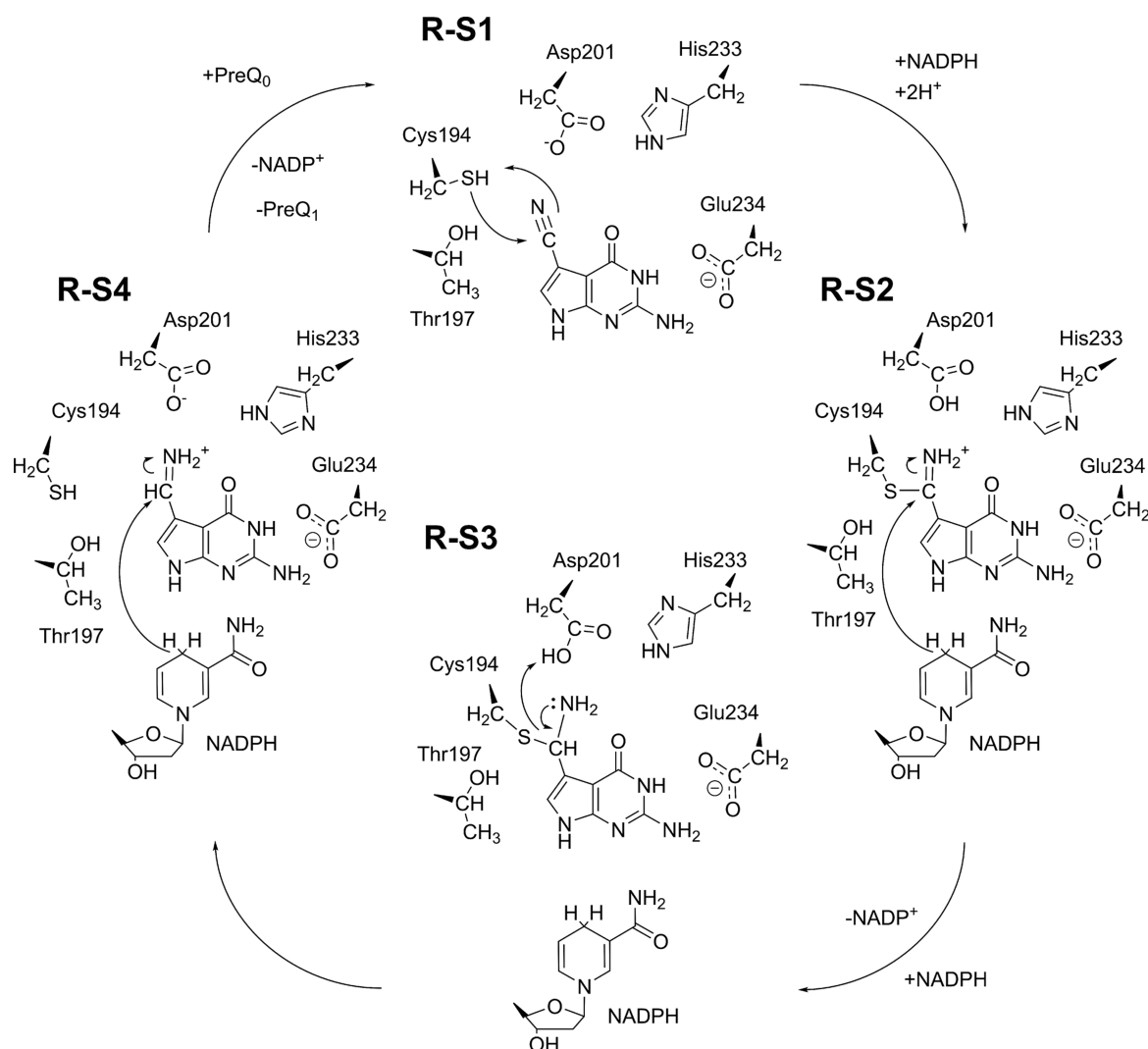
the exception of the first stage, the validity of which is well supported by the experimental observation of the thioimide intermediate, the catalytic mechanism of the enzyme remains to be fully established. In addition, the precise role of His233, the identities of the residues that donate protons to the nitrile group, and the protonation states of residues and the substrate along the reaction pathway are unknown.

In this paper, we report the results of our QM/MM computational study of *V. cholerae* QueF and propose a reaction path for the unique nitrile-reducing reaction catalyzed by QueF. We applied the ONIOM(B3LYP/6-311+g-(2d,2p):AMBER) method to a structural model of the enzyme, which contains the entire homodimer (two subunits) of *V. cholerae* QueF. This QM/MM methodology has been widely used so far to probe the catalytic mechanisms of a diversity of enzymes.<sup>22,23</sup> We computationally examined the four proposed stages that involve the formation of covalent intermediates and two NADPH-dependent reduction steps. The contribution of this work is 3-fold. First, it provides insight into the highly unusual mechanism of NADPH-dependent nitrile reduction. Second, together with existing experimental data, our computational results elucidate the catalytic roles of the residues in the active site. This information could be useful in future efforts to obtain nitrile-reducing biocatalysts by engineering nitrile reductases. Finally, the transition-state structures obtained from the calculations will be instrumental for the design of transition-state-like inhibitors for QueFs from pathogenic bacteria.

## 2. METHODS

We constructed a model for the nitrile reductase–cofactor–substrate complex using a high-resolution crystal structure (PDB code 3UXJ).<sup>18,24</sup> This structure contains two homodimers of *V. cholerae* nitrile reductase. We chose only one homodimer to proceed with the calculations. The homodimer has two active centers, each containing a molecule of the substrate. A single NADPH molecule is shared by the two active centers in such a way that the nicotinamide group is bound to one active center while the adenine group is bound to

Scheme 2. Schematic Representation of the Four Stages of the Reaction Catalyzed by Nitrile Reductase



the other. Only the active center that binds the nicotinamide group of NADPH should be able to catalyze the reaction; therefore, we focused on the reaction in this active center. The nicotinamide group is missing in the X-ray structure, but its positioning can be determined reasonably from the arrangement of the rest of the NADPH molecule. The missing atoms were appended to the model using GaussView software.<sup>25</sup>

Two systems were defined within the enzyme according to the ONIOM scheme:<sup>26–28</sup> a model system to which quantum mechanics (QM) and molecular mechanics (MM) are applied and a real system (entire homodimer) to which MM is applied. The model system contained the entire 7-cyano-7-deazaguanine substrate, the nicotinamide and ribose groups of NADPH, and the side chains of Asp201, Cys194, His233, Glu234, and Thr197. The side chains of aspartate, glutamate, cysteine, histidine, and threonine were included in the model system as acetate, methanethiol, 5-methylimidazole, and ethanol, respectively. The truncated bonds were capped with hydrogen link (H-link) atoms. In the real enzymatic reaction, NADPH goes in and out of the active center, and this unsettled nature of NADPH makes the size of the model system different in different stages. In addition, the protonation states of amino acid residues could also differ in different stages. Therefore, it is not possible to compare the energetics of different reaction

stages on an equal footing, but nevertheless, we can still compare the barrier heights for different stages. The largest model contained 92 atoms, and the smallest model contained 59 atoms (both including the H-link atoms). The model system was described with the B3LYP<sup>29,30</sup> DFT functional and the 6-31G(d)<sup>31</sup> basis set in geometry optimization calculations. The point charges of the atoms outside the model system were included in the QM Hamiltonian according to the electrostatic embedding scheme.

The real system was the entire homodimer, although the first 26 amino acids of each subunit, which were not present in the X-ray structure and might not be very important for the catalysis, were not included. The real system contained 8205 atoms in the models with NADPH and 8160 atoms in the models without NADPH. The Amber parm96 force field parameters,<sup>32</sup> as implemented in Gaussian 09,<sup>33</sup> were used for amino acid residues. For the NADPH molecule, we used the parameters of Holmberg et al.<sup>34–36</sup> We derived parameters for 7-cyano-7-deazaguanine using antechamber software,<sup>37</sup> which is part of the Amber10 suite of programs.<sup>38</sup> Antechamber chooses bonds, angles, and van der Waals parameters from the GAFF force field,<sup>39</sup> on the basis of the similarity to the structure being parametrized. Atomic point charges for the substrate were calculated using the HF/6-31G(d)<sup>40</sup> RESP (restrained electro-



Scheme 3. Schematic Representation of the First Stage of the Nitrile Reductase Reaction Mechanism: Formation of the Covalent Intermediate between the Substrate and Cys194

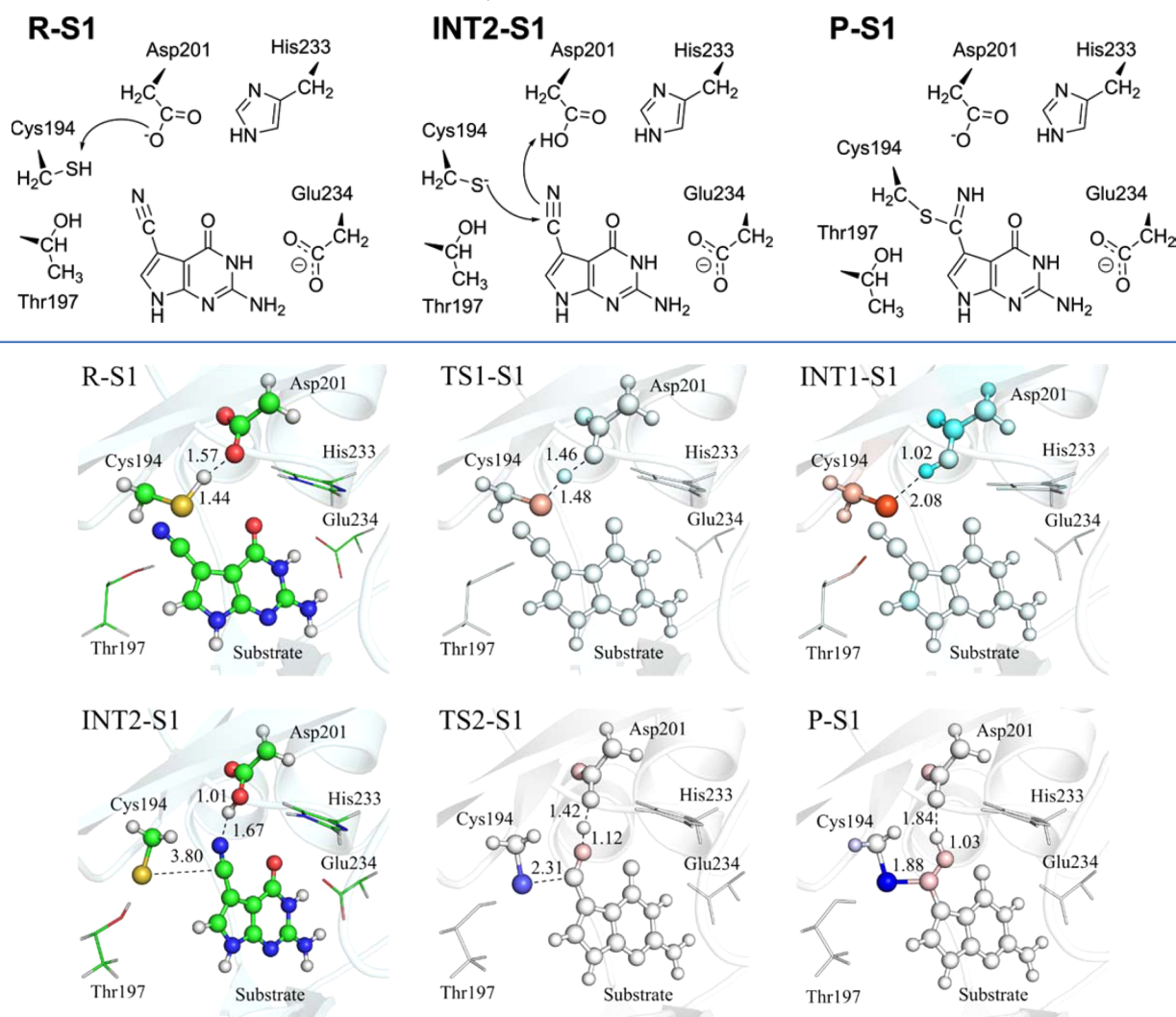


**Figure 2.** Optimized structures for the first stage of the nitrile reductase reaction mechanism. Only the QM-layer atoms are explicitly shown in the pictures. The coloring of TS1-S1, INT1-S1, TS2-S1, and P-S1 represents the difference of point atomic charges between that state and the previous minima. The red color means that the atom became more negatively charged, and the blue color indicates that the atom became more positively charged.

static potential) method,<sup>41</sup> to preserve the consistency with the Amber force field used for the protein.

The potential energy surface was roughly explored first by using appropriate internal coordinates. Subsequently, all minimum-energy states and transition states were optimized without imposing any constraints on either of the two layers. Frequency calculations were done to confirm the absence of imaginary frequencies in minimum-energy states and the existence of only one imaginary frequency in transition states. Values for zero-point-energy and free-energy corrections were also computed, and the latter were used to compute free energy values. Hence, free energies reported here are evaluated by frequency calculations, but not by structural sampling. In order to improve the accuracy of the QM description, single-point energy calculations were performed at a higher level of theory, using B3LYP/6-311+G(2d,2p).<sup>42–44</sup> Atomic charges were calculated with the Charge Model 5 (CMS) extension of the Hirschfeld scheme,<sup>45</sup> as implemented in Gaussian, and the CMS charges were used to understand how the charge

distributions change during reactions. All calculations were carried out using Gaussian 09 software.<sup>33</sup> PyMOL,<sup>46</sup> VMD (visual molecular dynamics),<sup>47</sup> and GaussView<sup>25</sup> were used as visualization tools.

### 3. RESULTS AND DISCUSSION

In the following sections, we present and discuss the four individual stages of the reaction mechanism of nitrile reductase (see Scheme 2). In particular, we will analyze the activation and reaction free energies, relevant geometry parameters, and charge reorganization modes along the reaction path. The intermediates and transition states in the pathway as well as other alternative pathways were subjected to close scrutiny using QM/MM calculations.

**3.1. Catalytic Mechanism. 3.1.1. Stage 1: Formation of a Covalent Intermediate.** Prior to the reduction of the nitrile group via the first hydride transfer from NADPH, a C–S bond is formed by the nucleophilic attack of the nitrile group of preQ<sub>0</sub> by Cys194. Formation of this covalent intermediate is

**Table 1. Relevant Interatomic Distances (in Å) for the First Stage of the Nitrile Reductase Mechanism: Formation of the Covalent Intermediate**

	R-S1	TS1-S1	INT1-S1	INT2-S1	TS2-S1	P-S1
nitrile C–nitrile N	1.16	1.16	1.16	1.16	1.19	1.25
nitrile C–Cys194 S	3.88	3.92	3.98	3.80	2.31	1.88
nitrile N–Asp201 H	4.72	4.74	4.93	1.67	1.12	1.03
Thr197 H–Cys194 S	2.70	2.61	2.24	2.17	2.17	2.27
Asp201 H–Asp201 O	1.57	1.46	1.02	1.01	1.42	1.84
Cys194 S–Cys194 H	1.44	1.48	2.08	4.96	3.71	3.01
His233 H–Asp201 O	1.97	2.00	2.28	2.27	2.02	2.07

supported by the observation of the thioimide intermediate, and the covalent-bond formation is known to be independent of the presence of NADPH.<sup>17,20</sup> For this reason, we did not include NADPH in the model for this reaction stage. Scheme 3 describes in detail the reaction steps in this stage, and the optimized structures of all stationary states are depicted in Figure 2. Tables 1 and 2 summarize the key interatomic distances and the charge distributions for these species, respectively.

**Table 2. Absolute Atomic Charges Grouped by Residues for the First Stage of the Nitrile Reductase Mechanism: Formation of the Covalent Intermediate<sup>a</sup>**

	R-S1	TS1-S1	INT1-S1	INT2-S1	TS2-S1	P-S1
substrate	-0.26	-0.26	-0.26	-0.12	-0.15	-0.21
Asp201	-0.69	-0.58	-0.20	-0.11	-0.50	-0.77
Cys194	-0.20	-0.31	-0.62	-0.74	-0.34	-0.06
His233	-0.14	-0.13	-0.09	-0.09	-0.13	-0.13
Thr197	-0.01	-0.02	-0.13	-0.23	-0.18	-0.12

<sup>a</sup>Only QM residues whose charge changes significantly are included. The charge of the thiol proton was divided into halves and distributed between Cys194 and Asp201 in the first transition state and between Asp201 and the substrate in the second transition state.

In the reactant state of the first stage (R-S1), all of the residues in the active site take on their normal protonation states: Asp201 and Glu234 are deprotonated and negatively charged, while His233, Cys194, Thr197, and the substrate are neutral. The first stage is initiated by a proton transfer from the thiol group of Cys194 to Asp201, which leads to the formation of an intermediate (INT1-S1). This proton transfer reaction involves a very early transition state; thus, the positions of the proton in R-S1 and in the transition state (TS-S1) are nearly the same, with the S–H distances being (1.44; 1.48; 2.08) Å and the H–O distances of the aspartate carboxylic group being (1.57; 1.46; 1.02) Å, where the three numbers in parentheses correspond to the distances for R-S1, TS-S1, and INT1-S1, respectively. The hydroxyl group of Thr197 is likely to play an important role in stabilizing the negatively charged thiolate form of Cys194. As the proton transfer progresses, the distance between hydroxyl and the sulfur decreases ( $r(\text{H}-\text{S}) = (2.70; 2.61; 2.24)$  Å). On the other hand, the interaction between one of the carboxylic oxygen atoms of Asp201 and the proton on the  $\epsilon$  nitrogen of His233 is weakened slightly ( $r(\text{O}-\text{H}) = (1.97; 2.00; 2.28)$  Å), likely because Asp201 is no longer negatively charged after the proton transfer. The free energy barrier for this proton transfer process is very small (0.8 kcal/mol), and the free energy of reaction is  $-3.5$  kcal/mol. Hence, the state containing ionized Cys194, which was formed as a

result of the proton transfer process, is more stable than the state containing ionized Asp201 and neutral Cys194.

In the proton-transfer step, Asp201 gains a positive charge of 0.49 (charge ( $Q$ ) =  $(-0.69; -0.58; -0.20)$ ), which comes mostly from Cys194 ( $Q = (-0.20; -0.31; -0.62)$ ). Thr197 and His233 also contribute to this new charge distribution by accepting a small amount of negative charge from the cysteine and a small amount of positive charge from Asp201. As can be seen in Figure 2, the negative charge that Cys194 gains is localized primarily on the sulfur atom, and the negative charge of Thr197 is concentrated mostly on the hydroxyl proton. In contrast, the calculation revealed that the newly developed positive charge on Asp201 and His233 is delocalized over their side chains.

The geometry of INT1-S1 is not optimum for the nucleophilic attack of the thiolate on the nitrile carbon atom. In order for the intermediate to proceed to the next reaction stage, the active site needs to undergo a significant conformational change to form the INT2-S1 state. The conformational change is thermodynamically favorable, because INT2-S1 is calculated to be 9.3 kcal/mol more stable than INT1-S1. In INT2-S1, Cys194 and Asp201 are closer to the  $-\text{CN}$  group and thus are in better positions for the next step of the reaction. The carboxylic oxygen atoms of Asp201 are located very far from the nitrogen atom of the nitrile ( $r(\text{H}-\text{N}) = 4.93$  Å) in INT1-S1, but the carboxylic oxygen atoms are positioned just next to the nitrogen atom in INT2-S1 ( $r(\text{N}-\text{H}) = 1.67$  Å) within a hydrogen-bonding distance. The conformational change to INT2-S1 alters the charge distribution in a manner that is more favorable for the subsequent nucleophilic attack: Cys194 and Thr197 become more negative and thus more nucleophilic, whereas the carbon center of the nitrile group becomes more positive.

The last step of this reaction stage involves the formation of a transition state (TS2-S1) for the nucleophilic addition reaction and a covalent thioimide intermediate (P-S1). In the thioimide intermediate, the substrate  $\text{preQ}_0$  becomes covalently tethered to the enzyme via Cys194. The C–S distances are (3.80; 2.31; 1.88) Å for INT2-S1, TS2-S1, and P-S1, respectively. Additionally, our calculations suggest that Asp201 is a general acid catalyst, since the carboxylic proton of Asp201 is transferred to the nitrogen atom of the nitrile group ( $r(\text{N}-\text{H}) = (1.67; 1.12; 1.03)$  Å). After the formation of the thioimide intermediate, the N–C triple bond is converted to a double bond ( $r(\text{N}-\text{C}) = (1.16; 1.19; 1.25)$  Å). The interaction between His233 and Asp201 residues is restored to that in the initial conformation, when Asp201 loses its proton to become negatively charged again.

During the C–S bond formation, Asp201 and Cys194 are seen to undergo the largest changes in charge distribution within the active center. Asp201 becomes negatively charged as

it donates its proton to the substrate, while Cys194 loses about the same amount of negative charge when it becomes covalently linked to the substrate. Close inspection of the atomic charges shows that the sulfur atom of Cys194 exhibits a significant change in electron density. The negative charge is lost from Cys194 predominantly through the sulfur atom. The loss of positive charge from Asp201 occurs through the leaving carboxylic proton, since the charge of all its atoms (including the proton) barely changes. As for the substrate, the nitrile group is responsible for accommodating most of the electronic density that is transferred to the substrate.

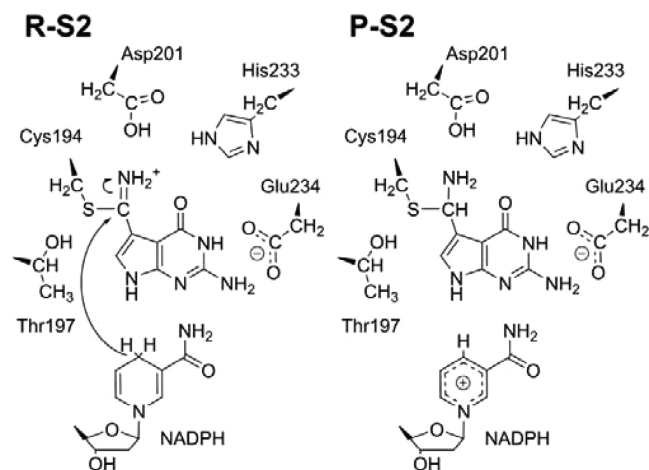
With respect to INT2-S1, the free energy barrier for this step is 19 kcal/mol and the free energy of reaction is 13.7 kcal/mol, whereas relative to the initial reactants, the barrier and reaction energy are 6.2 and 0.9 kcal/mol, respectively.

**3.1.2. Stage 2: First Hydride Transfer.** The second stage of the catalytic mechanism involves the reduction of the thioimide intermediate by a hydride from the cosubstrate NADPH. To reduce the thioimide intermediate (P-S1) generated from the first stage, an NADPH molecule and two protons must be supplied to the reaction center (Scheme 2). These protons originate most probably from the surrounding aqueous environment, since there is no suitable residue in the vicinity that could possibly act as proton donors. The overall charge of the active center decreases by 2 after the addition of the NADPH (4− charge) and the two protons (1+ charge each).

We examined a few possibilities concerning the protonation states of the nitrile group and Asp201. One possible mechanism involves the donation of a proton from Asp201 to the neutral nitrile group during hydride transfer. However, the energetics of this mechanism does not agree with the experimental  $k_{\text{cat}}$  or typical catalytic barriers. More information about this alternative mechanism is given in the [Supporting Information](#).

Another mechanism, which involves protonation of the thioimide intermediate, seems to be more reasonable energetically. For the reactant state of this more reasonable mechanism (R-S2), the carboxyl group of Asp201 and the nitrogen atom of the thioimide are first protonated (see Scheme 4). The nicotinamide group of NADPH now occupies the previously empty space of the active center and is positioned side by side with the substrate (see Figure 3). The

**Scheme 4. Schematic Representation of the Second Stage of the Nitrile Reductase Mechanism: Hydride Transfer from the First NADPH Molecule to the Nitrile Group**



hydride transfer reaction occurs in a single step, and the distances between the transferring hydride and the hydride-accepting carbon atom ( $r(\text{C}-\text{H})$ ) are 3.07, 1.55, and 1.09 Å for R-S2, TS-S2, and P-S2, respectively. Table 3 gives other relevant geometric parameters for this reaction stage. The distance between the hydride and the nicotinamide carbon increases accordingly ((1.11; 1.28; 2.69) Å). These values suggest that this stage involves an early transition state (TS1-S2), at which point the hydride is closer to the NADPH molecule (1.28 Å) than to the  $\text{C}=\text{NH}_2$  group (1.55 Å). At TS-S2, the angle subtended by these three atoms is large (171.3°). During the hydride transfer, the  $\text{C}=\text{N}$  double bond becomes a  $\text{C}-\text{N}$  single bond, and the  $\text{C}-\text{N}$  distance increases accordingly ( $r(\text{C}-\text{N}) = (1.33; 1.41; 1.47)$  Å). We also observe a few other minor structural changes that facilitate the hydride-transfer process. For example, the bond between the sulfur atom of Cys194 and the carbon atom of the  $\text{C}=\text{NH}_2^+$  group is elongated ( $r(\text{S}-\text{C}) = (1.76; 1.79; 1.86)$  Å) to accommodate the additional electronic density. The hydrogen bond between the nitrogen atom of  $\text{C}=\text{NH}_2^+$  and the carboxylic hydrogen of Asp201 is shortened and therefore strengthened ( $r(\text{N}-\text{H}) = (2.15; 1.70; 1.58)$  Å). The other hydrogen bond between the  $\epsilon$  nitrogen atom of His233 and the amine group of nicotinamide is also shortened ( $r(\text{N}-\text{H}) = (2.79; 2.04; 2.22)$  Å), suggesting that the slightly basic histidine residue plays a role in stabilizing the formation of the positive nicotinamide group. The activation free energy for this reaction step was calculated as 19.1 kcal/mol, and the free energy of reaction was −14.9 kcal/mol.

An analysis of the charge distribution along the reaction path provides some interesting clues about the origin of transition state stabilization. Differences in the atomic partial charges are shown in Figure 3. Table 4 shows the absolute atomic charges grouped by residues. Along the reaction path, the NADPH molecule loses one negative charge, which is compatible with the transfer of a hydride ( $Q = (-0.02, 0.38, 0.87)$ ). The initial and final negative charges of NADPH are not delocalized over other residues, indicating that both NADPH and  $\text{NADP}^+$  are relatively stable. The additional positive charge of  $\text{NADP}^+$  is uniformly distributed over the nicotinamide group, but some localization on the aromatic ring is observed. In contrast, the thioimide intermediate has only a partial positive charge of 0.55, in the R-S2 state. The rest of the positive charge is delocalized over Cys194, which is covalently bonded to the  $\text{C}=\text{NH}_2$  group, and over Glu234, which is now less negative. The differences in charge distributions among R-S2, TS-S2, and P-S2 allow us to identify which residues contribute significantly to the catalysis by accepting some of the negative charge of the hydride. In this case, Asp201 and Cys194 are important, becoming ca. 0.2 more negative along the reaction path. His233, Thr197, and Glu234 maintain roughly the same charge. Within the thioimide intermediate, the C and N atoms of the  $\text{C}=\text{NH}_2$  group accept more negative charges than the other atoms. The sulfur atom and the carboxylic oxygen atoms accept the negative charge to the greatest extent in Cys194 and Asp201, respectively.

**3.1.3. Stage 3: Cleavage of the C–S Bond.** Before the second hydride transfer, the  $\text{NADP}^+$  ion must be replaced with another NADPH molecule. We also assume that the covalent  $\text{C}-\text{S}$  bond must be broken to generate an imine intermediate. Although theoretically it is possible to generate the final amine product directly from the thiohemiaminal intermediate via an  $\text{S}_{\text{N}}2$  mechanism with the hydride as nucleophile, our study



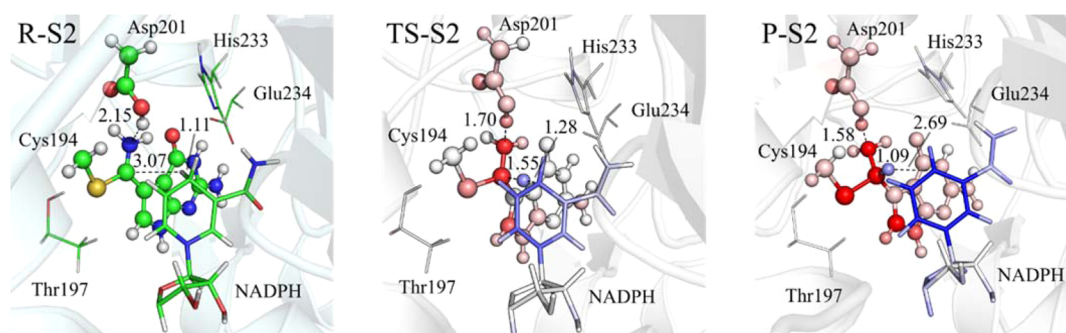


**Figure 3.** Optimized structures for the second stage of the nitrile reductase mechanism. Only the QM-layer atoms are explicitly shown in the pictures. The coloring of TS1-S2 and P-S2 represents the difference of point atomic charges between that state and the reactants. The red color means that the atom became more negatively charged, and the blue color indicates that the atom became more positively charged.

**Table 3. Relevant Interatomic Distances (in Å) and Angles (in deg) for the Second Stage of the Nitrile Reductase Reaction: First Hydride Transfer**

	R-S2	TS-S2	P-S2
nitrile C–nitrile N	1.33	1.41	1.47
nitrile C–Cys194 S	1.76	1.79	1.86
nitrile C–H <sup>−</sup>	3.07	1.55	1.09
NADPH C–H <sup>−</sup>	1.11	1.28	2.69
nitrile N–Asp201 H	2.15	1.70	1.58
His233 N–NADPH H	2.79	2.04	2.22
nitrile C–H <sup>−</sup> –NADPH C	136	171	156

**Table 4. Absolute Atomic Charges Grouped by Residues for the Second Stage of the Nitrile Reductase Mechanism: First Hydride Transfer<sup>a</sup>**

	R-S2	TS-S2	P-S2
NADPH	−0.02	0.38 <sup>b</sup>	0.87
substrate	0.55	0.30 <sup>b</sup>	0.04
Asp201	0.02	−0.10	−0.17
Cys194	0.10	0.06	−0.08

<sup>a</sup>Only QM residues whose charge changes significantly are included.

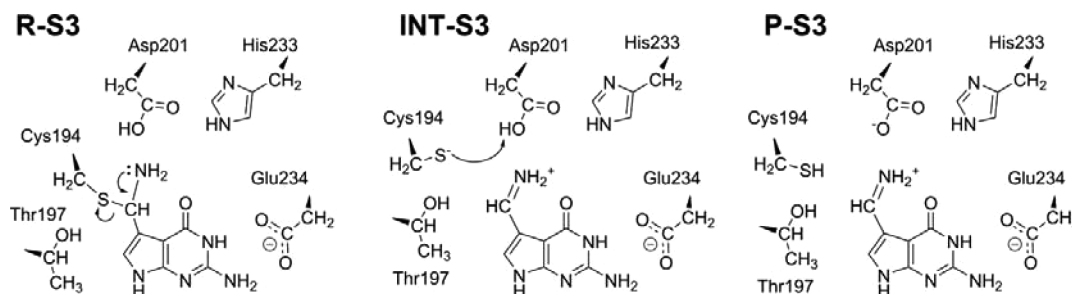
<sup>b</sup>We divided the charge of the hydride ion evenly between the NADPH and the substrate in the transition state.

suggested that this mechanism is not plausible because of the severe steric hindrance caused by the Cys194 residue. If the C–S bond is not broken first, Cys194 will sterically prohibit the nicotinamide moiety from approaching the covalent-attached intermediate. We studied this C–S bond-breaking process with NADPH bound in the active center. The presence of NADPH

could be important for two reasons. First, because the imine intermediate is prone to hydrolysis in the presence of a water molecule, the presence of NADPH might be crucial for protecting the imine from H<sub>2</sub>O and thereby safeguarding against formation of a side product. Second, NADPH may play a role in maintaining or preorganizing the active center in an optimal conformation and charge distribution. Scheme 5 depicts the individual steps from this stage, while Figure 4 shows the optimized reactant, transition state, and product structures for each step. The main interatomic distances and the charge distributions are included in Tables 5 and 6, respectively.

In the reactant state of this reaction (R-S3), the side chain of Asp201 is protonated while all other residues in the active center have their default protonation states. Apart from the change from NADP<sup>+</sup> to NADPH, there is no other significant change in the active center, in comparison with P-S2 in the first hydride-transfer reaction (stage 2). During the first step of this stage (from R-S3 via TS1-S3 to INT-S3), the bond between the sulfur atom of Cys194 and the carbon atom of the original nitrile group is broken ( $r(\text{C–S}) = (1.97; 2.39; 3.19)$  Å). It is the side chain of Asp201 that contributes most to the stabilization of the transition state by maintaining and gradually strengthening the hydrogen bond with the sulfur atom during this reaction step ( $r(\text{S–H}) = (2.27; 2.20; 2.09)$  Å). The hydroxyl group of Thr197 can also form a hydrogen bond with the sulfur atom, but only in the final intermediate state ( $r(\text{S–H}) = (4.64; 4.45; 2.49)$  Å). The change in bond order from 1 (C–N) to 2 (C=N) is apparent. Not only has the bond length decreased ( $r(\text{C–N}) = (1.42; 1.35; 1.30)$  Å) but also the nitrogen atom has changed its configuration from pyramidal sp<sup>3</sup>

**Scheme 5. Schematic Representation of the Third Stage of the Nitrile Reductase Reaction Mechanism: Breaking of the Covalent Intermediate between the Substrate and Cys194<sup>a</sup>**



<sup>a</sup>NADPH is present in the QM layer of this QM/MM model but is not shown here for simplicity.

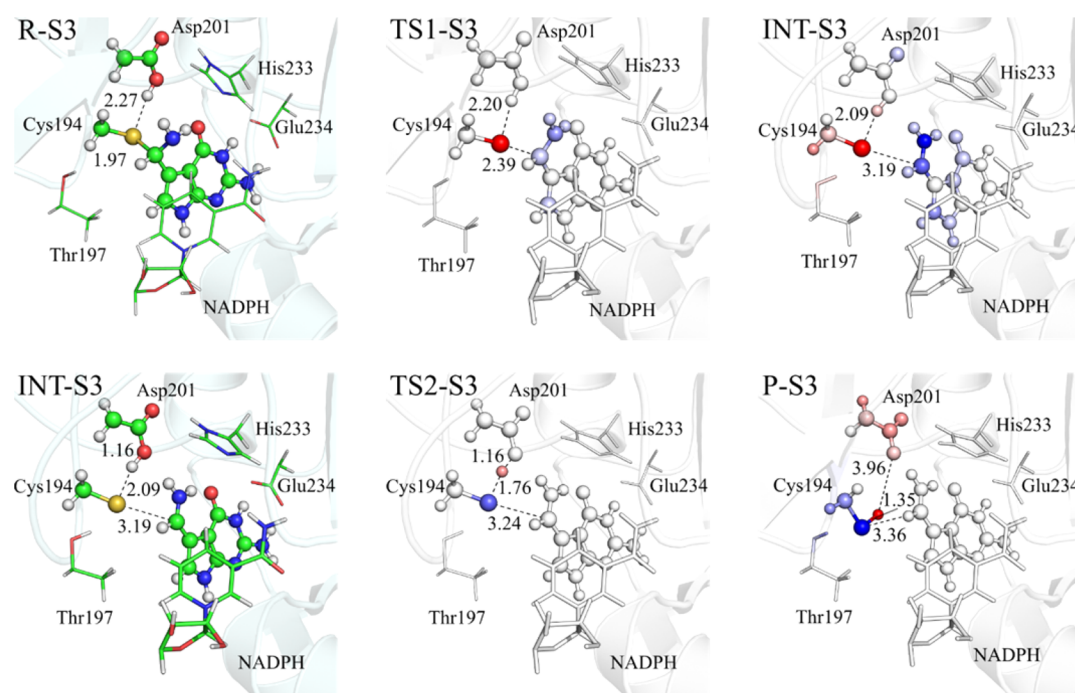


**Figure 4.** Optimized structures for the third stage of the nitrile reductase reaction mechanism. Only the QM-layer atoms are explicitly shown in the pictures. The coloring of TS1-S3, INT-S3, TS2-S3, and P-S3 represents the difference of point atomic charges between that state and the previous minima. The red color means that the atom became more negatively charged, and the blue color indicates that the atom became more positively charged. The structure of INT is shown twice, but in different representations.

**Table 5. Relevant Interatomic Distances (in Å) for the Third Stage of the Nitrile Reductase Reaction: Breaking of the Covalent Intermediate**

	R-S3	TS1-S3	INT1-S3	TS2-S3	P-S3
nitrile C–nitrile N	1.42	1.35	1.30	1.30	1.30
nitrile C–Cys194 S	1.97	2.39	3.19	3.24	3.36
Asp201 O–nitrile H	3.67	3.43	2.19	1.94	1.62
Thr197 H–Cys194 S	4.64	4.45	2.49	2.57	3.78
Asp201 H–Asp201 O	1.00	1.01	1.03	1.16	3.96
Asp201 H–Cys194 S	2.27	2.20	2.09	1.76	1.35
His233 H–Asp201 O	2.06	1.98	2.12	2.07	1.99

**Table 6. Absolute Atomic Charges Grouped by Residues for the Third Stage of the Nitrile Reductase Mechanism: Breaking of the Covalent Intermediate<sup>a</sup>**

	R-S3	TS1-S3	INT1-S3	TS2-S3	P-S3
substrate	0.04	0.26	0.58	0.58	0.54
Asp201	−0.10	−0.12	−0.14	−0.35 <sup>b</sup>	−0.68
Cys194	−0.09	−0.33	−0.58	−0.37 <sup>b</sup>	−0.05
His233	−0.11	−0.11	−0.09	−0.10	−0.14
Thr197	0.04	0.04	−0.06	−0.03	0.04

<sup>a</sup>Only QM residues whose charge changes significantly are included.

<sup>b</sup>We divided the charge of the Asp201 proton into halves and distributed the split charges to Cys194 and Asp201 at TS2-S3.

to planar  $sp^2$  (Figure 4). The activation free energy for this step is 4.9 kcal/mol, and this step is slightly exergonic, with its free energy of reaction being  $-2.3$  kcal/mol.

Calculated charge distributions (Table 6) clearly show that the charge polarization increases as the distance between the sulfur and carbon atoms becomes greater. In the thiohemiaminal intermediate, the substrate carries a positive charge of  $+0.58$ , while Cys194 has a negative charge of  $-0.58$ . All other

residues in the active center remain neutral. In terms of the atomic charges (Figure 4), the sulfur harbors most of the newly developed negative charge in Cys194, while the positive charge of the reactant is localized to the largest extent on the  $N_{C-NH_2}$  atom, followed by the  $C_{C-NH_2}$  atom and then the 7-deazapurine moiety. Asp201 is not completely inert, as the noticeable change in its overall charge suggests. A slight polarization between its carboxylic proton and the deprotonated carboxylic oxygen atom can be observed in the INT-S3 state (see Figure 4)

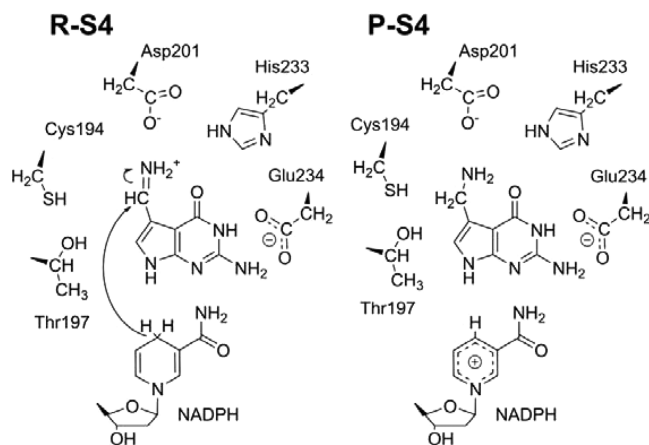
In the second step of this stage, the negatively charged Cys194 accepts a proton from Asp201. The transition state (TS2-S3) is a very early one, at which the Asp201 proton has moved only slightly from the carboxylic oxygen atom, as can be seen from the  $r(O-H)$  distances of (1.03; 1.16; 3.96) Å for INT-S3, TS2-S3, and P-S3, respectively. The distance between the proton and the sulfur atom decreases accordingly ( $r(S-H) = (2.09; 1.76; 1.35)$  Å). The other two interactions, i.e., the interactions between Thr197 and Cys194 and between Asp201 and the nitrile, change significantly along this path, especially in a late stage: the hydroxyl group of Thr197 moves away from the sulfur atom, now that the sulfur is no longer negatively charged ( $r(S-H) = (2.49; 2.57; 3.78)$  Å), and the now negatively charged Asp201 carboxylic group becomes tightly bound to the positive nitrile group of the substrate ( $r(O-H) = (2.19; 1.94; 1.62)$  Å). The energy of TS2-S3 is 1.7 kcal/mol relative to INT1-S3 and  $-0.6$  kcal/mol relative to R-S3. This step has large reaction energies of  $-24.3$  and  $-22.9$  kcal/mol relative to INT1-S3 and P-S3, respectively. This substantial reaction energy may not be accounted for by the proton transfer alone, but it may be largely due to the formation of a favorable ionic bond between Asp201 and the  $-NH_2$  group.



The charge variations at TS2-S3 are rather small (see TS2-S3 in Table 6 and Figure 4) and are solely concentrated on the sulfur atom of Cys194 and the carboxylic proton of Asp201. However, in the product state, the charge delocalization is more extensive. Asp201 has a negative charge of  $-0.68$ , which is dispersed over its side chain, and Cys194 is now neutral. Thr197, another residue located in the active site, also accepts some charge from the sulfur atom.

**3.1.4. Stage 4: Second Hydride Transfer.** The last step of the reaction involves the transfer of a second hydride from NADPH to the imine intermediate. The reactant state for this stage is essentially the same as P-S3 from the previous stage. The negatively charged Asp201 interacts strongly with the positively charged imine group of the substrate, and all of the other residues are in their normal protonation states. In our calculations, although the structures of R-S4 and P-S3 are not exactly the same because they are located in different energy minima, the main geometrical parameters in the active center are very similar. Scheme 6 illustrates the reaction steps of this

**Scheme 6. Fourth Stage of the Nitrile Reductase Mechanism: Hydride Transfer from the Second NADPH Molecule to the Nitrile Group**



stage, and Figure 5 shows the optimized structures of all stationary states. Tables 7 and 8 summarize the key interatomic distances and the charge distributions, respectively.

The hydride transfer from the nicotinamide group of NADPH to the imine group of the intermediate occurs in a single step. The  $r(\text{C}(\text{nitrile})-\text{H})$  values are (2.50; 1.28; 1.11) Å for R-S4, TS-S4, and P-S4, respectively, and the  $r(\text{C}(\text{NADPH})-\text{H})$

**Table 7. Relevant Interatomic Distances (in Å) and Angles (in deg) for the Fourth Stage of Nitrile Reduction: Second Hydride Transfer**

	R-S4	TS-S4	P-S4
nitrile C–nitrile N	1.30	1.38	1.47
nitrile C–Cys194 S	3.33	3.46	3.39
nitrile C–hydride	2.50	1.28	1.11
NADPH C–hydride	1.10	1.50	2.72
nitrile H–Asp201 O	1.70	1.91	2.10
His233 N–NADPH amide H	2.97	2.12	2.13
His233 H–Asp201 O	2.52	2.37	2.16
nitrile C–hydride–NADPH C	141	154	108

**Table 8. Absolute Atomic Charges Grouped by Residues for the Fourth Stage of the Nitrile Reductase Mechanism: Second Hydride Transfer<sup>a</sup>**

	R-S4	TS-S4	P-S4
NADPH	-0.01	0.46 <sup>b</sup>	0.83
substrate	0.53	0.09 <sup>b</sup>	-0.22
Asp201	-0.75	-0.79	-0.80
Cys194	-0.06	-0.06	-0.08
His233	-0.07	-0.03	-0.04

<sup>a</sup>Only QM residues whose charge changes significantly are included.  
<sup>b</sup>We divided the charge of the hydride ion into halves and distributed them to the NADPH and the substrate at TS-S4.

(NADPH)–H) values are (1.10; 1.50; 2.72) Å. Thus, at the transition state (TS-S4), the hydride is closer to the carbon atom of imine than to the nicotinamide carbon of NADPH. This late transition state is in contrast to the early transition state of the first hydride transfer, which explains why the barrier is lower for the first hydride transfer. The arrangement of these three atoms is also less linear than in the first hydride transfer reaction: angle (141; 154; 108)°, compared with (136; 171; 156)° for the first reduction. The C=N double bond of the intermediate is reduced to yield an N–H single bond during the reaction, which is evident from the increase in bond length ( $r(\text{C}-\text{N}) = (1.30; 1.38; 1.47)$  Å and the change in hybridization of N from planar  $sp^2$  to pyramidal  $sp^3$ . The interaction between Asp201 and the nitrile hydrogen is significantly weakened as the reaction progresses ( $r(\text{H}-\text{O}) = (1.70; 1.91; 2.10)$  Å). On the other side of the carboxylic group of Asp201, the interaction between the oxygen and the NH moiety of His233 becomes stronger ( $r(\text{O}-\text{H}) = (2.52; 2.37; 2.16)$  Å). Concomitantly, the interaction between the  $\delta$

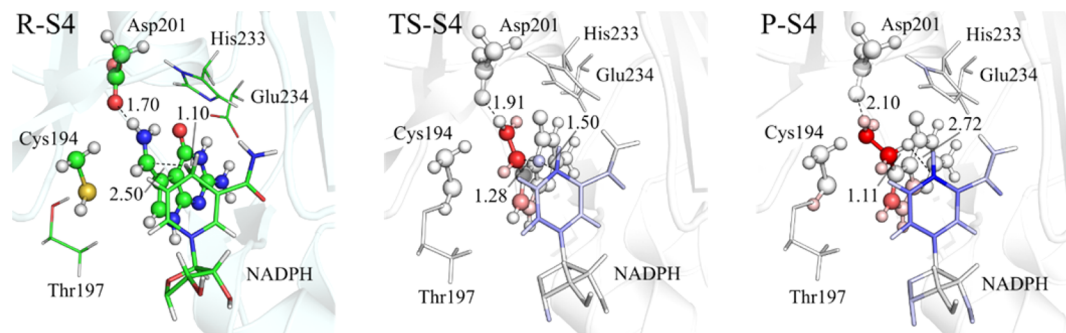


**Figure 5. Optimized structures for the fourth stage of the nitrile reductase mechanism. Only the QM-layer atoms are explicitly shown in the pictures. The coloring of TS1-S4 and P-S4 represents the difference of point atomic charges between that state and the reactants. The red color means that the atom became more negatively charged, and the blue color indicates that the atom became more positively charged.**

nitrogen of His233 and the amide group of NADPH is also strengthened ( $r(\text{N-H}) = (2.97; 2.12; 2.13) \text{ \AA}$ ). Hence, it seems that Asp201 also helps stabilize the newly formed positive charge on NADPH, though not as efficiently as the imine group does. The activation free energy of this step is 20.8 kcal/mol, and the free energy of reaction is 10.8 kcal/mol.

The change in charge distribution is consistent with the way the geometrical parameters change. The NADPH molecule becomes increasingly positive with the progress of the reaction ( $Q = (-0.01; 0.46; 0.83)$ ), while the substrate receives most of the negative charge ( $Q = (0.53; 0.09; -0.22)$ ). The overall charge of the rest of the residues hardly changes. In Figure 5, we can see that the positive charge of  $\text{NADP}^+$  is well delocalized over the nicotinamide ring, while the charge on the substrate is mostly concentrated on the imine group. Nevertheless, other parts of NADPH and the substrate also undergo slight variations in the charge. Some of the negative charge of the substrate goes to the five-membered ring of the 7-deazapurine, and the amide and ribose groups of the NADPH also receive some amounts of positive charge. The interaction between the amide group of NADPH and His233 seems to be significantly strengthened as the reaction progresses. The negatively charged Asp201 is likely to stabilize the accumulating charge in the amide group indirectly through this bridging histidine residue.

**3.2. Summary and Comparison with Experimental Kinetic Data.** The free energy profiles for the four reaction stages obtained from our calculations are summarized in Figure 6. The barriers for stages 1–4 are 19.0, 19.1, 4.9, and 20.8 kcal/

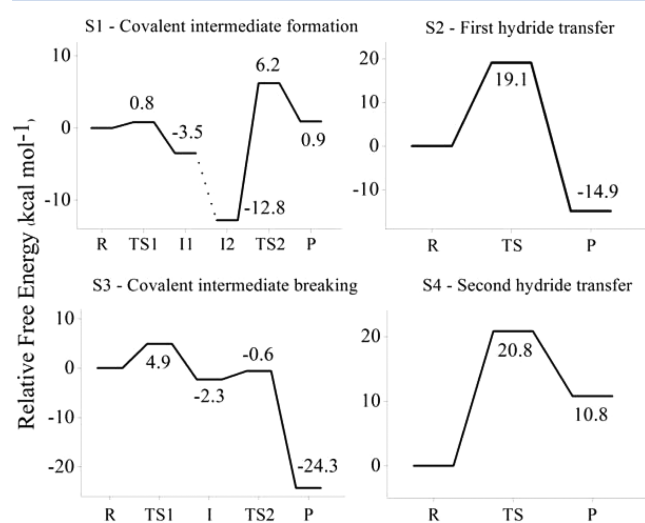


**Figure 6.** Free energy profiles for the four stages of the nitrile reductase reaction.

mol, respectively. The second hydride transfer occurring in stage 4 constitutes the rate-limiting step of the overall reaction. Stage 3 was found to be the process associated with the lowest kinetic barriers.

The above calculations identified the rate-limiting step of the catalytic reaction of nitrile reductase as the second hydride transfer via TS-S4, which has an energy barrier of 20.8 kcal/mol. The barrier for the first hydride transfer via TS-S2 is almost as high, the value being 19.1 kcal/mol. These values agree well with the available data on the experimental turnover of nitrile reductase enzymes. Although there is no published value of  $k_{\text{cat}}$  for the *V. cholerae* enzyme, to the best of our

knowledge, we can use the  $k_{\text{cat}}$  values for the enzymes of *B. subtilis*,<sup>20,21</sup> *E. coli*,<sup>13,14</sup> and *G. kaustophilus*.<sup>12</sup> The enzyme turnovers of these organisms are  $0.011 \text{ s}^{-1}$  (at  $30 \text{ }^\circ\text{C}$ ),  $0.12 \text{ s}^{-1}$  (at  $30 \text{ }^\circ\text{C}$ ), and  $0.065 \text{ s}^{-1}$  (at  $55 \text{ }^\circ\text{C}$ ), respectively. These values are converted to free energy barriers of 20.5, 19.0, and 20.7 kcal/mol, according to transition state theory. The turnover number for *V. cholerae* should be comparable, since the active centers of the four enzymes are very similar.

The rate-limiting step of the formation of the covalent intermediate is the nucleophilic attack of the negative sulfur atom of Cys194 on the substrate (TS2-S1), and the free energy barrier for this step is 19.0 kcal/mol. Since the formation of the covalent intermediate is not dependent on NADPH, it is possible to stop the reaction at P-S1 by not adding the NADPH to the reaction mixture. The trapping of the thioimide intermediate is demonstrated in an experimental study,<sup>17</sup> and the rate of the thioimide formation was estimated to be on the order of  $2 \text{ s}^{-1}$ , which corresponds to a barrier of 17.8 kcal/mol. This value agrees very well with our calculations.

In stage 4, P-S4 is less stable than the previous intermediate. Since the reaction is expected to be spontaneous, there must be additional reaction steps or contributions to the energy that lead to an overall exergonic reaction. The contribution could come from the entropic energy gain arising from the release of the  $\text{preQ}_1$  and  $\text{NADP}^+$  molecules from the active center. The contribution of this stabilization effect will be even more prominent if the concentration of these two molecules in solution is low. Structural reorganization of the enzyme active center, and the difference in energy for the binding of  $\text{preQ}_1$  and  $\text{NADP}^+$ , may also affect the stability of the product, which were not accounted for in our model. A similar trend was also observed for stage 1. In this stage, the unstable product may be stabilized when the NADPH enters the active center.

**3.3. Roles of the Catalytic Residues.** Our computational results and the available experimental data allow us to obtain a clear picture of the roles of the residues in the active site during the course of catalysis. The most prominent residue in this regard is Cys194. Early experimental results for the *B. subtilis* QueF<sup>20</sup> showed that the presence of the  $\text{preQ}_0$  prevented Cys194 (Cys55 in *B. subtilis*) from reacting with iodoacetamide, indicating that a covalent intermediate is presumably formed between  $\text{preQ}_0$  and Cys194. More recently, crystal structures showed unambiguously the existence of such a thioimide intermediate.<sup>17</sup> Site-directed mutagenesis studies also confirmed that the enzyme loses its activity without this cysteine residue.<sup>13</sup> Although the essential role of Cys194 in the reaction has been established experimentally, this mechanistic study provided detailed insight into how Cys194 is covalently linked to the substrate in the first stage of the reaction. We also showed that the C–S bond formation is essential for the transfer of the first hydride ion in stage 2. Further, before the first reduction, the thioimide intermediate should be positively charged as the result of prior protonation and have a double-bond character at the C–N bond. In the first hydride transfer, this configuration is possible only after the covalent-bond formation with Cys194. However, as discussed above, the C–S bond impedes the second hydride transfer; therefore, it must be broken in the third stage of the reaction.

It was also shown by mutagenesis studies that Asp201 is essential for the enzyme activity.<sup>13</sup> Our calculations suggest that Asp201 should be involved in all four stages of the nitrile reductase reaction. In the first stage, Asp201 accepts a proton from the thiol group of Cys194 and later donates the proton to

the nitrile nitrogen atom of the substrate. In the second stage, Asp201 plays an indirect role in stabilizing the positively charged intermediate through very strong hydrogen bonding that allows Asp201 to delocalize some of the negative charge resulting from hydride transfer. In the third stage, Asp201 protonates the negatively charged sulfur atom of Cys194, which arises from the cleavage of the covalent C–S bond. Finally, in the fourth stage, Asp201 stabilizes the positively charged transition state and intermediate.

Because of its proximity to the nitrile group, one may assume that His233 acts as a general-base/acid catalyst during the catalysis. However, its role in the catalysis seems to be nonessential. His233 interacts either with Asp201 or with the substrate, but only via nonbonding interactions without any proton transfer. Glu234 is another residue that mutagenesis results have indicated as important for the catalytic mechanism.<sup>13</sup> Together with the X-ray crystallographic data,<sup>15–17</sup> our computational study suggests that the major role of Glu234 is to bind and orient the pre $Q_0$  substrate, rather than act as a general base/acid catalyst. Finally, we found Thr197 to be important in the first stage of the reaction, because it stabilizes the negatively charged sulfur atom before the nucleophilic attack on the substrate.

#### 4. CONCLUSIONS

We investigated the catalytic mechanism of *V. cholerae* QueF nitrile reductase by using the method of QM/MM calculations. We obtained the kinetic barriers for the four individual steps and elucidated the crucial conformational changes required for bond-breaking and -forming events. The results together yield fresh insight into the catalytic mechanism of the highly unique process of biological nitrile reduction. The fourth stage (i.e., the second hydride transfer) was identified as the rate-limiting step of the reaction, with a free energy barrier of 20.8 kcal/mol. This result is in accordance with the turnover rate of the QueF homologues from various organisms. Overall, the mechanism we presented here is consistent with X-ray structural observations, kinetic data, and site-directed mutagenesis results. We hope that the detailed catalytic mechanism will assist the current efforts of enzyme engineering and inhibitor design.

#### ■ ASSOCIATED CONTENT

##### Supporting Information

The Supporting Information is available free of charge on the ACS Publications website at DOI: 10.1021/acscatal.5b00528.

XYZ coordinates of the QM atoms in the optimized geometries, alternative mechanism for the first hydride transfer stage, and RMSDs of the protein low layer along the reaction (PDF)

#### ■ AUTHOR INFORMATION

##### Corresponding Authors

\*E-mail for P.A.F.: [paferman@fc.up.pt](mailto:paferman@fc.up.pt).

\*E-mail for Z.-X.L.: [zxliang@ntu.edu.sg](mailto:zxliang@ntu.edu.sg).

\*E-mail for H.H.: [hirao@ntu.edu.sg](mailto:hirao@ntu.edu.sg).

##### Notes

The authors declare no competing financial interest.

#### ■ ACKNOWLEDGMENTS

This work is supported by the GSK-EDB Green Manufacturing award to Z.-X.L. H.H. acknowledges a Nanyang Assistant Professorship and the computational resources at the High-

Performance Computing Centre at Nanyang Technological University. This work has been funded by the Fundação para a Ciência e Tecnologia (FCT) through grant EXCL/QE-QCOM/0394/2012 (M.J.R. and P.A.F.). A.J.M.R. thanks the FCT for a postdoctoral scholarship (SFRH/BPD/94883/2013).

#### ■ REFERENCES

- (1) Iwata-Reuyl, D. *Bioorg. Chem.* **2003**, *31* (1), 24.
- (2) El Yacoubi, B.; Bailly, M.; de Crécy-Lagard, V. *Annu. Rev. Genet.* **2012**, *46*, 69.
- (3) Iwata-Reuyl, D. *Curr. Opin. Chem. Biol.* **2008**, *12* (2), 126.
- (4) Durand, J. M. B.; Dagberg, B.; Uhlin, B. E.; Björk, G. R. *Mol. Microbiol.* **2000**, *35* (4), 924.
- (5) Prasad, S.; Bhalla, T. C. *Biotechnol. Adv.* **2010**, *28* (6), 725.
- (6) Kobayashi, M.; Nagasawa, T.; Yamada, H. *Trends Biotechnol.* **1992**, *10*, 402.
- (7) Kobayashi, M.; Shimizu, S. *Nat. Biotechnol.* **1998**, *16* (8), 733.
- (8) Yeom, S.-J.; Kim, H.-J.; Oh, D.-K. *Enzyme Microb. Technol.* **2007**, *41* (6–7), 842.
- (9) Martinková, L.; Vejvoda, V.; Kaplan, O.; Kubáč, D.; Malandra, A.; Cantarella, M.; Bezouška, K.; Křen, V. *Biotechnol. Adv.* **2009**, *27* (6), 661.
- (10) Yang, L.; Koh, S. L.; Sutton, P. W.; Liang, Z.-X. *Catal. Sci. Technol.* **2014**, *4* (9), 2871.
- (11) Domínguez de María, P. *ChemCatChem* **2011**, *3* (11), 1683.
- (12) Wilding, B.; Winkler, M.; Petschacher, B.; Kratzer, R.; Glieder, A.; Klempier, N. *Adv. Synth. Catal.* **2012**, *354* (11–12), 2191.
- (13) Wilding, B.; Winkler, M.; Petschacher, B.; Kratzer, R.; Egger, S.; Steinkellner, G.; Lyskowski, A.; Nidetzky, B.; Gruber, K.; Klempier, N. *Chem. - Eur. J.* **2013**, *19* (22), 7007.
- (14) Moeller, K.; Nguyen, G.-S.; Hollmann, F.; Hanefeld, U. *Enzyme Microb. Technol.* **2013**, *52* (3), 129.
- (15) Swairjo, M. A.; Reddy, R. R.; Lee, B.; Van Lanen, S. G.; Brown, S.; de Crécy-Lagard, V.; Iwata-Reuyl, D.; Schimmel, P. *Acta Crystallogr., Sect. F: Struct. Biol. Cryst. Commun.* **2005**, *61* (10), 945.
- (16) Kim, Y.; Zhou, M.; Moy, S.; Morales, J.; Cunningham, M. A.; Joachimiak, A. *J. Mol. Biol.* **2010**, *404* (1), 127.
- (17) Chikwana, V. M.; Stec, B.; Lee, B. W. K.; de Crécy-Lagard, V.; Iwata-Reuyl, D.; Swairjo, M. A. *J. Biol. Chem.* **2012**, *287* (36), 30560.
- (18) Kim, Y.; Zhang, R.; Gu, M.; Anderson, W. F.; Joachimiak, A. CSIGD, deposited in PDB: <http://www.rcsb.org/pdb>.
- (19) Reader, J. S.; Metzgar, D.; Schimmel, P.; Crécy-Lagard, V. de J. *Biol. Chem.* **2004**, *279* (8), 6280.
- (20) Lee, B. W. K.; Van Lanen, S. G.; Iwata-Reuyl, D. *Biochemistry* **2007**, *46* (44), 12844.
- (21) Lanen, S. G. V.; Reader, J. S.; Swairjo, M. A.; de Crécy-Lagard, V.; Lee, B.; Iwata-Reuyl, D. *Proc. Natl. Acad. Sci. U. S. A.* **2005**, *102* (12), 4264.
- (22) Vreven, T.; Byun, K. S.; Komaromi, I.; Dapprich, S.; Montgomery, J. A.; Morokuma, K.; Frisch, M. J. *J. Chem. Theory Comput.* **2006**, *2* (3), 815.
- (23) Chung, L. W.; Hirao, H.; Li, X.; Morokuma, K. *Wiley Interdiscip. Rev.-Comput. Mol. Sci.* **2012**, *2* (2), 327.
- (24) Berman, H. M.; Westbrook, J.; Feng, Z.; Gilliland, G.; Bhat, T. N.; Weissig, H.; Shindyalov, I. N.; Bourne, P. E. *Nucleic Acids Res.* **2000**, *28* (1), 235.
- (25) Dennington, R.; Keith, T.; Millam, J. *GaussView, version 5*; Semichem Inc., Shawnee Mission, KS, 2009.
- (26) Maseras, F.; Morokuma, K. *J. Comput. Chem.* **1995**, *16* (9), 1170.
- (27) Svensson, M.; Humbel, S.; Froese, R. D. J.; Matsubara, T.; Sieber, S.; Morokuma, K. *J. Phys. Chem.* **1996**, *100* (50), 19357.
- (28) Dapprich, S.; Komaromi, I.; Byun, K. S.; Morokuma, K.; Frisch, M. J. *J. Mol. Struct.: THEOCHEM* **1999**, *461*, 1.
- (29) Becke, A. D. *J. Chem. Phys.* **1993**, *98* (7), 5648.
- (30) Lee, C.; Yang, W.; Parr, R. G. *Phys. Rev. B: Condens. Matter Mater. Phys.* **1988**, *37* (2), 785.



- (31) Ditchfield, R.; Hehre, W. J.; Pople, J. A. *J. Chem. Phys.* **1971**, *54* (2), 724.
- (32) Cornell, W. D.; Cieplak, P.; Bayly, C. I.; Gould, I. R.; Merz, K. M.; Ferguson, D. M.; Spellmeyer, D. C.; Fox, T.; Caldwell, J. W.; Kollman, P. A. *J. Am. Chem. Soc.* **1995**, *117* (19), 5179.
- (33) Frisch, M.; Trucks, G.; Schlegel, H.; Scuseria, G.; Robb, M.; Cheeseman, J.; Scalmani, G.; Barone, V.; Mennucci, B.; Petersson, G.; Nakatsuji, H.; Caricato, M.; Li, X.; Hratchian, H.; Izmaylov, A.; Bloino, J.; Zheng, G.; Sonnenberg, J.; Hada, M.; Ehara, M.; Toyota, K.; Fukuda, R.; Hasegawa, J.; Ishida, M.; Nakajima, T.; Honda, Y.; Kitao, O.; Nakai, H.; Vreven, T.; Montgomery, J. A., Jr; Peralta, J.; Ogliaro, F.; Bearpark, M.; Heyd, J.; Brothers, E.; Kudin, K.; Staroverov, V.; Kobayashi, R.; Normand, J.; Raghavachari, K.; Rendell, A.; Burant, J.; Iyengar, S.; Tomasi, J.; Cossi, M.; Rega, N.; Millam, J.; Klene, M.; Knox, J.; Cross, J.; Bakken, V.; Adamo, C.; Jaramillo, J.; Gomperts, R.; Stratmann, R.; Yazyev, O.; Austin, A.; Cammi, R.; Pomelli, C.; Ochterski, J.; Martin, R.; Morokuma, K.; Zakrzewski, V.; Voth, G.; Salvador, P.; Dannenberg, J.; Dapprich, S.; Daniels, A.; Farkas; Foresman, J.; Ortiz, J.; Cioslowski, J.; Fox, D. *Gaussian 09 Revision D.01*; Gaussian Inc., Wallingford, CT, 2009.
- (34) Ryde, U. *Proteins: Struct., Funct., Genet.* **1995**, *21* (1), 40.
- (35) Ryde, U. *Protein Sci. Publ. Protein Soc.* **1995**, *4* (6), 1124.
- (36) Holmberg, N.; Ryde, U.; Bülow, L. *Protein Eng., Des. Sel.* **1999**, *12* (10), 851.
- (37) Wang, J.; Wang, W.; Kollman, P. A.; Case, D. A. *J. Mol. Graphics Modell.* **2006**, *25* (2), 247.
- (38) Case, D. A.; Darden, T. A.; Cheatham, T. E.; Simmerling, C. L.; Wang, J.; Duke, R. E.; Luo, R.; Crowley, M.; Walker, R. C.; Zhang, W. *Amber 10*; University of California, 2008.
- (39) Wang, J. M.; Wolf, R. M.; Caldwell, J. W.; Kollman, P. A.; Case, D. A. *J. Comput. Chem.* **2004**, *25* (9), 1157.
- (40) Roothaan, C. C. J. *Rev. Mod. Phys.* **1951**, *23* (2), 69.
- (41) Bayly, C.; Cieplak, P.; Cornell, W.; Kollman, P. *J. Phys. Chem.* **1993**, *97* (40), 10269.
- (42) McLean, A. D.; Chandler, G. S. *J. Chem. Phys.* **1980**, *72* (10), 5639.
- (43) Clark, T.; Chandrasekhar, J.; Spitznagel, G. W.; Schleyer, P. V. *R. J. Comput. Chem.* **1983**, *4* (3), 294.
- (44) Frisch, M. J.; Pople, J. A.; Binkley, J. S. *J. Chem. Phys.* **1984**, *80* (7), 3265.
- (45) Marenich, A. V.; Jerome, S. V.; Cramer, C. J.; Truhlar, D. G. *J. Chem. Theory Comput.* **2012**, *8* (2), 527.
- (46) *The PyMOL Molecular Graphics System, Version 1.6.0.0*; Schrodinger LLC, 2010.
- (47) Humphrey, W.; Dalke, A.; Schulten, K. *J. Mol. Graphics* **1996**, *14* (1), 33.